Bull. Inst. Chem. Res., Kyoto Univ., Vol, 49, No. 5, 1971

Growth and Electrical Properties of V_nO_{2n-1} (n=3, 4, ..., 8) Single Crystals

Koichi NAGASAWA*, Yoshichika BANDO** and Toshio TAKADA**

Received October 6, 1971

Single crystals of the intermediate vanadium oxides between V_2O_3 and VO_2 with the general formula V_nO_{2n-1} (n=3, 4, ..., 8) were grown by the chemical transport reaction using $TeCl_4$ as a transport agent. The reactions were carried out in sealed tubes. The sizes of the crystals produced were about 1~10 mm. The temperature dependence of magnetic susceptibility, electrical resistivity and thermoelectric power were measured on single crystals. V_3O_5 having monoclinic structure was n-type semiconductor at the temperature ranging from 130°K to room temperature. On V_4O_7, V_5O_9, V_6O_{11} and V_8O_{15} having triclinic sturcture, metal-semiconductor transitions occurred at 250°K, 135°K, 177°K and 70°K, respectively. These transition temperatures were coincident with those of the anomaly in magnetic susceptibility. V_7O_{13} having triclinic structure showed metallic conduction below room temperature.

INTRODUCTION

There have been many investigations on the intermediate vanadium oxides between V_2O_3 and VO_2. These phases, which are expressed by general formula V_nO_{2n-1} (n=3, 4, ..., 8), were found by Andersson[1] and except V_3O_5 commonly called Magnéli phases after the main investigator. Burdese[2] and Grossman *et al.*[3] confirmed Andersson's results. Kosuge[4] studied the phase relation between V_2O_3 and V_2O_5 in a closed system and so proposed the phase diagram combined with the results which Kachi and Roy[5] obtained. In addition to the phase studies mentioned above, Katsura *et al.*[6,7] measured the equilibrium oxygen pressure for each phase at 1600°K and 1800°K. Furthermore, Okinaka *et al.*[8] recently determined the stability range of each phase as a function of the oxygen pressure and temperature from 800°K to 1600°K.

The structures of Magnéli phases have been investigated by S. Andersson *et al.*[9,10] Based on the crystal structure of Ti_5O_9, one of titanium Magnéli phases, S. Andersson showed that the structures could be explained by introducing periodic shear plane to the rutile structure. The structure of V_3O_5 has been determined by Åsbrink *et al.*[11]

Moreover, there has been recently considerable interest in the magnetic and electrical properties on these phases. Kosuge[4] measured the temperature dependence of magnetic susceptibility and showed that the magnetic susceptibilities of V_3O_5, V_4O_7, V_5O_9 and V_6O_{11} had the large anomalies at 133°K, 250°K, 139°K and 177°K,

* 長沢紘一：Now at Central Research Laboratory, Mitsubishi Electric Corp., Amagasaki, Hyogo.
** 坂東尚周，高田利夫：Laboratory of Solid State Chemistry, Institute for Chemical Research, Kyoto University, Uji, Kyoto.

respectively. Mössbauer effect measurements[4] revealed that the phase transformation in V_4O_7 and V_5O_9 was not a usual magnetic transition from paramagnetic to antiferromagnetic but a crystallographic transformation like VO_2.[12] Kachi *et al.*[13] measured the temperature dependence of electrical resistivity using sintered samples of these phases, and observed small anomaly on only V_5O_9 at about 140°K. Single crystals of V_nO_{2n-1} were necessary in order to investigate further the electrical properties. However, single crystals of V_nO_{2n-1} except V_3O_5[14] have not been obtained, because each phase is stable in the narrow range of oxygen pressure at high temperature, as shown in Fig. 1.[8]

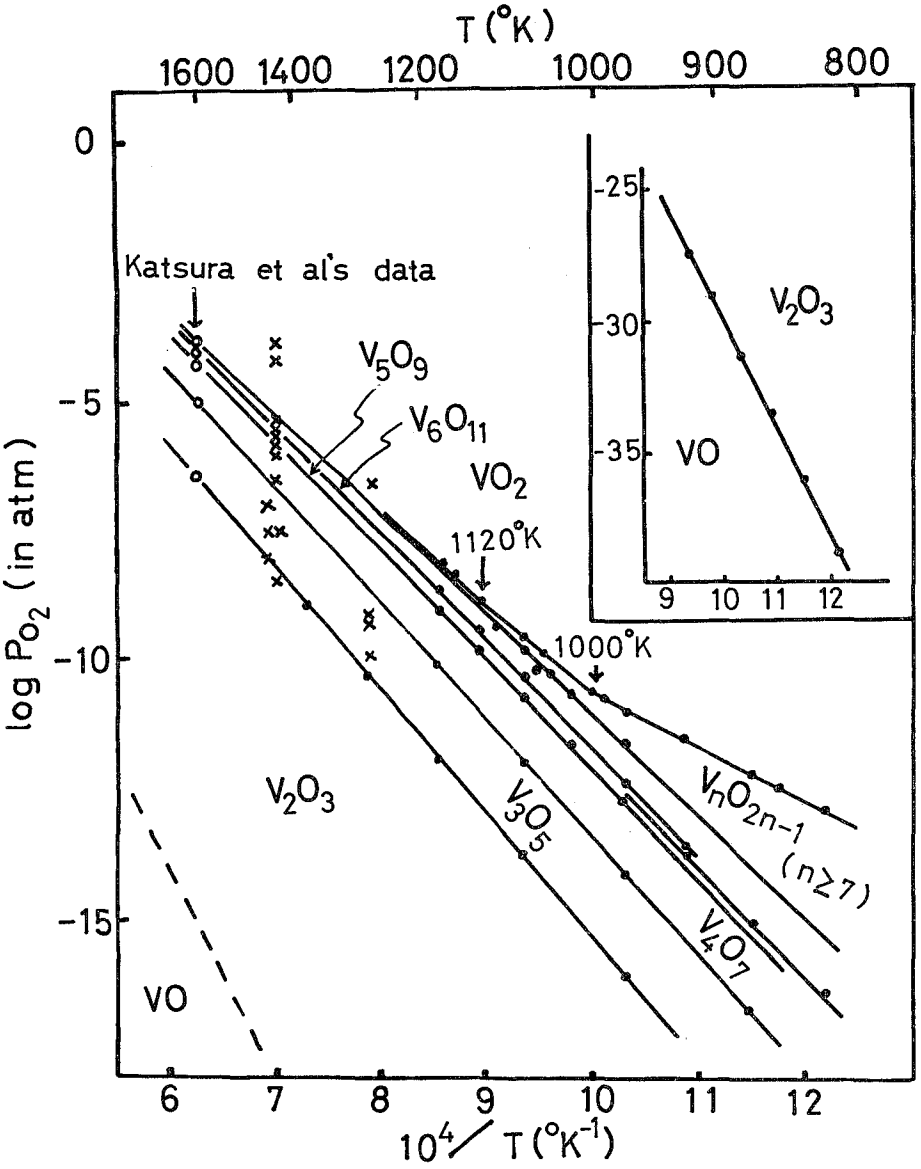

Fig. 1. Plot of log P_{O_2} versus $10^4/T°K$ for the V_2O_3, V_3O_5, V_4O_7, V_5O_9, V_6O_{11}, V_7O_{13} and VO_2 respectively.[8]

Chemical transport reaction in a closed system may be suitable for growing single crystals of these phases which are stable under such conditions, because the equilibrium oxygen pressure of an oxide can be automatically controlled in a tube. Recently, Niemyski *et al.*[15] prepared highly pure single crystals of TiO_2 by chemical transport reaction using $TeCl_4$. Bando *et al.*[16] also prepared VO_2 single crystals by the same method. Moreover, single crystals of V_nO_{2n-1} have been recently grown by Nagasawa *et al.*[17~19,24,25] In the experiment, the postulated reaction of the type,

$$V_nO_{2n-1}(s)+\left(n-\frac{1}{2}\right)TeCl_4(g) \rightleftarrows (n-2)VCl_4(g)+2VCl_3(g)+\left(n-\frac{1}{2}\right)TeO_2(g)$$

was used, where (s) shows solid state and (g) gaseous state.

The present paper aims to examine the conditions for the preparation of V_nO_{2n-1} single crystals to investigate the electrical properties from the measurements of electrical resistivity and thermoelectric power, and aims to find the relation of the phase transformation and the structure having periodic shear plane.

Some parts of this investigation were already reported in short note.[17~26] In this paper, the detailed results are reviewed and summarized.

EXPERIMENTALS

1. Growth procedures

The sealed tube for the chemical transport reaction was made by the following way. V_nO_{2n-1} powder of about 1 gram as the starting material was loaded into the end of transparent silica tube of 13 mm in diameter and 170 mm in length. In the case of V_8O_{15}, VO_2 and V_6O_{11} mixed in mole ratio of 1.9 and 2.0 were used as the starting one. And then $TeCl_4$ powder as a transport agent was added into the silica tube in the dry box. After the tube was evacuated to 10^{-6} mmHg, it was sealed off. The tube was inserted in the horizontal electric furnace, where the source zone with the starting material was kept at 1050°C and the crystallization zone at 950°C. The tube was heated for 72 hr. The reaction was stopped by quenching the tube in water. The tube was broken out, and the crystals at the crystallization zone were removed from the wall of silica glass. Chemical transport yielded many crystals which were 0.5~10 mm in length and 0.5~2 mm in width. The crystals were washed in diluted aqueous HCl solution, and $TeCl_4$ was dissolved. And then crystals were washed in water and dried. In order to measure the transport rate, the crystals obtained at the crystallization zone were weighed. The V/O ratios of the crystals obtained were volumetrically determined by Zinc-Amalgam method.[27] Spectroscopic analysis for starting material V_3O_5 and the crystals obtained was performed.

2) Phase identifications and measurements

The phases of crystals were identified by x-ray diffraction analysis and measurements of magnetic susceptibility. The x-ray powder patterns were taken using Ni-filtered

Cu-K radiation. The magnetic susceptibility was measured with many crystals of 0.5~5 mm in size. In order to confirm the crystal to be a single crystal, Laue photograph was taken of the growth plane for a crystal of 5~10 mm in width, using W radiation. The crystal system and lattice constant of V_nO_{2n-1} single crystals were determined by the x-ray precession photographs and 4-circle x-ray diffractometer, using Mo-K radiation.

The measurements of electrical resistivity were carried out along the growth axis of a rod-like crystal by means of four point method using a d. c. potentiometer. On V_3O_5, the measurements were done, in the directions parallel and perpendicular to the growth axis, by four point method and two point method.

To measure the thermoelectric power, both ends of a rod-like crystal were firmly clamped to two copper blocks between which it was about 5 mm. One copper block was jointed to a heater. Cu-AuCo thermocouple and copper wire were attached to both ends of a crystal using silver paste. The temperature difference between both ends was measured by the two thermocouples. At the same time, the difference of potential between both copper wires was measured by micro voltage meter. The temperature difference between both ends of a crystal was kept to be 2°~4°C by controlling the current of heater.

RESULT AND DISCUSSION

1) Crystal growth

Crystals obtained at the crystallization zone were bright and black in color, rod-like or plate-like in shape and up to 12 mm in size. Figure 2 shows the photograph of the crystals obtained. Table 1 shows the representative transport conditions for V_3O_5, V_4O_7, V_5O_9, V_6O_{11}, V_7O_{13} and V_8O_{15}, transport rates, phases of the starting

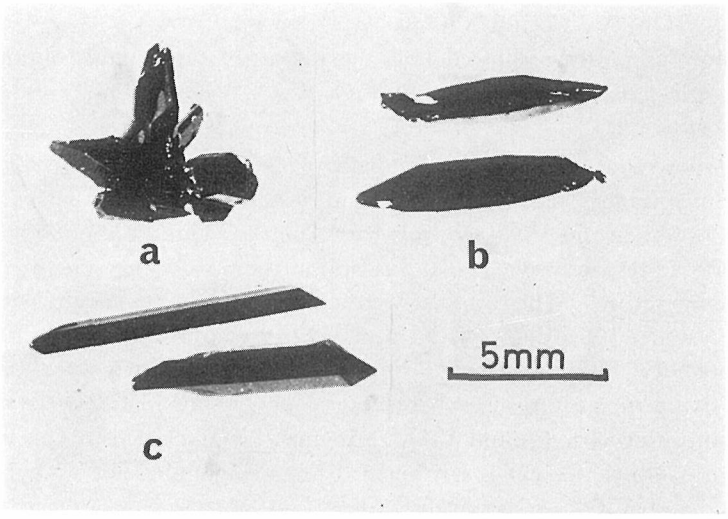

Fig. 2. Photographs of typical crystals obtained in the crystallization zone.
(a) V_7O_{13} (b) V_3O_5 (c) V_6O_{11}

Table 1. Representative Conditions for Growth of V_nO_{2n-1} Single Crystals and Phases of Products.

Run No.	Starting material (before reaction)	$TeCl_4$ weight (mg/cc)	Transport rate (mg/hr)	Starting material (after reaction)	Crystals obtained (after reaction)	Results of chemical analysis for crystals obtained. (x in VO_x) Observed	calculated
A-1	V_3O_5	2	0.4	V_3O_5	V_3O_5**	1.65	1.67
A-2	V_3O_5	4	1.0	V_3O_5*	V_3O_5**	—	—
A-3	V_3O_5	6	3.6	V_3O_5*	V_3O_5**	—	—
A-4	V_3O_5	8	4.1	V_3O_5*	V_3O_5**	—	—
B-1	V_4O_7	8	4.3	V_4O_7*	V_4O_7**	1.74	1.75
C-1	V_5O_9	8	4.4	V_5O_9*	V_5O_9**	1.80	1.80
C-2	V_5O_9	8	4.3	$V_5O_9+V_6O_{11}$*	$V_5O_9+V_6O_{11}$**	1.81	—
D-1	V_6O_{11}	8	4.5	V_6O_{11}	V_6O_{11}**	1.82	1.83
E-1	V_7O_{13}	8	4.1	V_7O_{13}	V_7O_{13}**	1.86	1.86
F-1	$VO_2+V_6O_{11}$ (1.9 : 1)	8	4.0	V_8O_{15}*	V_8O_{15}**,***	1.87	1.88
F-2	$VO_2+V_6O_{11}$ (2.0: 1)	8	4.5	—	$V_8O_{15}+V_9O_{17}$***	—	—

The phase was identified by x-ray analysis*, x-ray analysis and magnetic susceptibility measurement** or x-ray precession photograph***.

materials present at the source zone after reaction and of the crystals obtained at the crystallization zone and results of chemical analysis.

The transport rate for each phase increased with amount of $TeCl_4$ in the tube. For instance, the rate of V_3O_5 increased with amount of $TeCl_4$ per unit volume of the tube, as shown in Table 1. $TeCl_4$ of 8 mg per unit volume yielded the largest crystals in comparison with less amount. The crystal growth under the amount above 8 mg of $TeCl_4$ per unit volume was not done because the tube exploded owing to high pressure of $TeCl_4$ gas. The explosion was also found in the growth experiment of V_4O_7, V_5O_9, V_6O_{11}, V_7O_{13} and V_8O_{15}.

X-ray powder patterns showed that the phases of the crystals obtained in run A-4, B-1, C-1, D-1, E-1 and F-1 were of V_3O_5, V_4O_7, V_5O_9, V_6O_{11}, V_7O_{13} and V_8O_{15}, respectively.

Figure 3 shows the temperature dependence of magnetic susceptibility for the crystals obtained. Susceptibility of V_3O_5 crystals had a smooth peak at 130°K[17] but, that of V_4O_7, V_5O_9, V_6O_{11} and V_8O_{15} crystals had a marked kink at about 250°K, 135°K, 170°K and 70°K, respectively.[18,19,24] Susceptibility of V_7O_{13} crystals increased with decreasing temperature. These results were approximately coincident with Kosuge's results[4] for V_3O_5, V_4O_7, V_5O_9, V_6O_{11} and V_7O_{13} except V_8O_{15}. The susceptibility *vs* temperature curve for a sample consisting of two phases had two kinks corresponding to the transition temperature of each phase. The crystals in C-2 were found to be two phases consisting of V_5O_9 and V_6O_{11}. It must be concluded by this method that the crystals in A-4, B-1, C-1, D-1, E-1 and F-1 are a single phase of V_3O_5, V_4O_7, V_5O_9, V_6O_{11}, V_7O_{13} and V_8O_{15}, respectively.

As shown in Table 1, the V/O ratio of the single crystals determined by chemical analysis approximately agreed with the value expected from V_nO_{2n-1}.

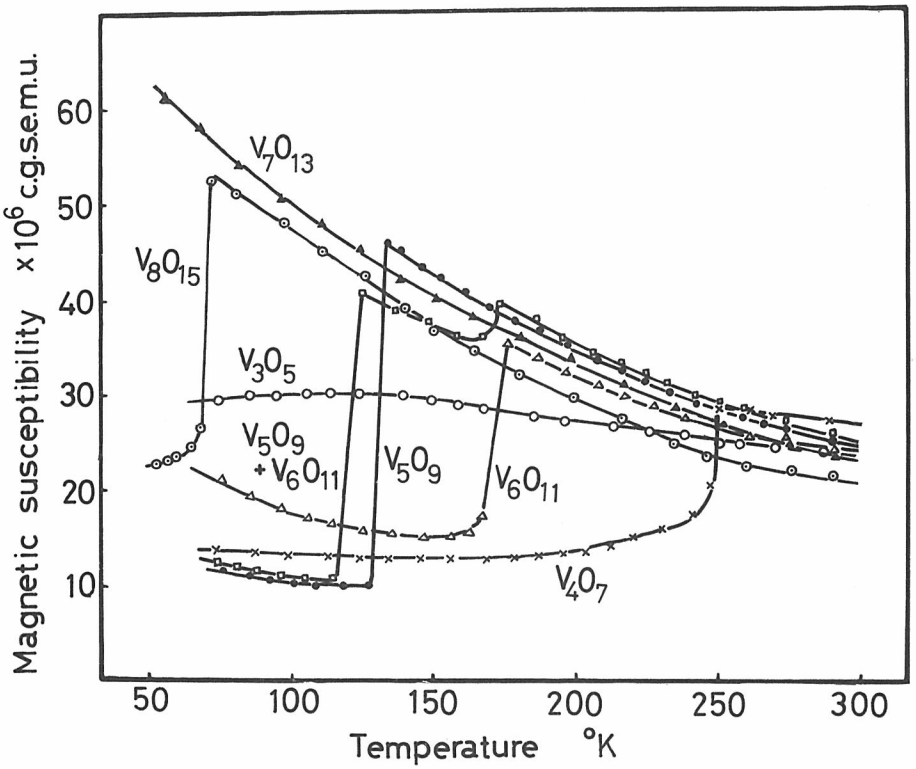

Fig. 3. Temperature dependence of the magnetic susceptibility of V_nO_{2n-1} crystals.

X-ray Laue photograph seemed to show that the crystal was single. However, it was often observed by precession photograph that crystals were twinned. Figure 4 shows the precession photograph of a V_8O_{15} single crystal. The precession photo-

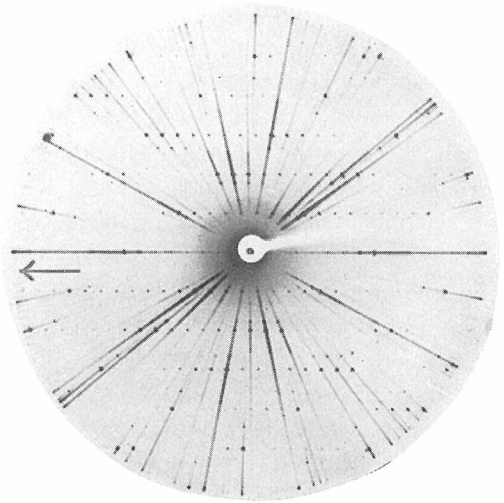

Fig. 4. Precession photograph of V_8O_{15}. The superstructure reflections which divide the interval of the main reflections into eight parts are found along the direction shown by the arrows.

Table 2. Crystal System and Lattice Constant in Reduced Lattice. Åsbrink *et al's*[11] and Andersson *et al's*[10] Results are shown in the Bracked.

	sys	a(A)	b(A)	c(A)	α	β	γ	V(A^3)
V_3O_5	mono.	9.854 (9.86)	5.040 (5.04)	6.990 (6.99)	90 (90)	109.5 (109.5)	90 (90)	327.3 (327.4)
V_4O_7	tric.	6.778 (6.72)	7.007 (7.01)	5.504 (5.51)	109.2 (109.0)	104.6 (104.6)	64.2 (64.3)	220.5 (220.1)
V_5O_9	tric.	7.005 (6.99)	8.353 (8.34)	5.470 (5.47)	104.9 (104.9)	109.0 (109.0)	69.5 (69.5)	279.7 (278.7)
V_6O_{11}	tric.	6.998 (6.99)	9.569 (9.56)	5.448 (5.44)	100.6 (100.7)	108.9 (108.9)	90.0 (90.1)	338.5 (337.1)
V_7O_{13}	tric.	7.005 (7.00)	11.115 (11.11)	5.439 (5.43)	91.2 (91.1)	109.0 (108.9)	84.0 (84.1)	398.3 (397.4)
V_8O_{15}	tric.	7.02 (6.199)	13.10 (13.79)	5.42 (5.43)	95.7 (98.0)	109.5 (109.0)	100.2 (99.5)	456.0 (455.1)

graph revealed the existence of superstructure along the special direction. The interval of the main reflections was equally divided into eight parts along the special direction. Generally, the photographs of V_nO_{2n-1} except V_3O_5 showed the division of the interval of the main reflections into n parts. The crystal system and lattice constant were determined with 4-circle diffractometer. The lattices obtained above were reduced by using UTRDCL[28] and their results are shown in Table 2. The lattice constants which could be obtained by transforming Åsbrink *et al.*[11] and Andersson *et al*'s[10] lattices to the type of reduced lattice are shown in the brackets of Table 2 and approximately agreed with those obtained in this experiment. Therefore, it is considered that the crystal structures proposed by Andersson *et al.*[9] were reasonable. The lattice constants of V_3O_5 having monoclinic structure also agreed with those obtained by transforming Åsbrink *et al*'s[11] lattice to the reduced lattice. The detailed discussion on the crystallography of V_nO_{2n-1} based on the rutile structure will be given in other paper by Horiuchi *et al.*[29]

From the x-ray precession photographs, it is also concluded that the crystals obtained are single crystals of V_nO_{2n-1} (n=3, 4, ..., 8), respectively. However, in C-2, the crystals with two phases of V_5O_9 and V_6O_{11} were obtained using the starting material with a single phase. It must be considered that the starting material of V_5O_9 had been already oxidized in air, because single crystals with a single phase was generally obtained from starting material with a single phase. The stability range of V_5O_9 is very narrow, as shown in Fig. 1, and so the slight oxidization of starting material appears to cause the formation of V_6O_{11} with V_5O_9. The starting material corresponding to the composition of V_8O_{15}, VO_2 and V_6O_{11} mixed in mole ratio of 2.0, also yielded the crystals with two phases of V_8O_{15} and V_9O_{17}, as mentioned later. In the consideration of the oxidization, VO_2 and V_6O_{11} mixed in mole ratio of 1.9 were used as the starting material and single crystals of V_8O_{15} were obtained. This suggests that V_8O_{15} is stable only in the very narrow stability range of the equilibrium oxygen pressure. Each of V_nO_{2n-1} having in higher than 9 is considered to be stable only in the very narrow range of the equilibrium oxygen pressure at elevated temperature. Therefore, it should be noticed that single crystals of V_nO_{2n-1} (n>9) may

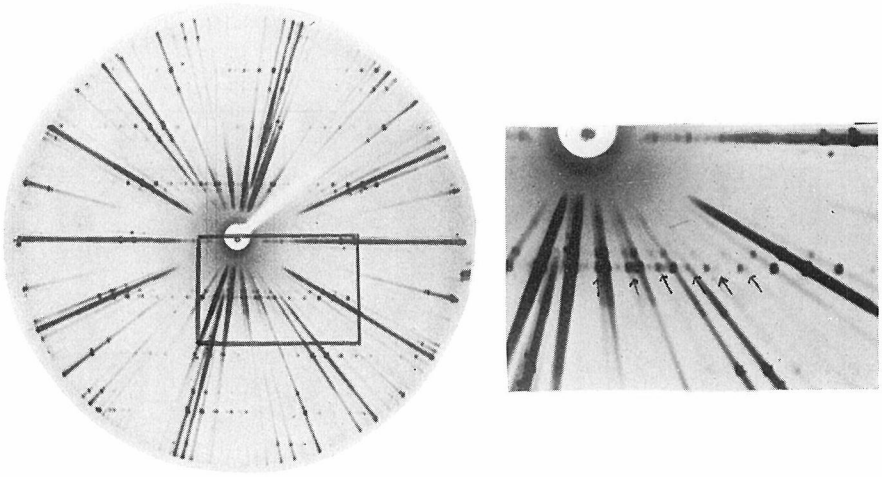

(a) (b)

Fig. 5. (a) Precession photograph showing the topotactic relation of V_8O_{15} and V_9O_{17}. (b) A part of the photograph is enlarged to show the reflections from the two phases. The weak spots of V_9O_{17} are indicated by arrows.

be prepared by protecting the strating material from being oxidized by air before reaction.

To examine the structure of the crystal with two phases, the precession photograph was taken of a crystal with two phases. In the precession photograph of a crystal in F-2, as shown in Fig. 5, the weak reflections which divide the interval of the main reflections into nine parts were observed in addition to the strong reflections, which divided the interval into eight parts, corresponding to V_8O_{15}. From these reflections it is apparent that V_9O_{17} topotaxially exists in the crystal of V_8O_{15}. As mentioned later, the temperature dependence of electrical resistivity of a crystal in C-2 shows the two anomalies corresponding to V_5O_9 and V_6O_{11} and two phases coexist in a crystal.

Table 3. Spectroscopic Analysis of Vanadium Oxides

Element	Starting material V_3O_5 (ppm)	Single crystals V_3O_5 (ppm)	Single crystals V_4O_7 (ppm)
Fe	50	50	50
Co	—	—	—
Ni	100	100	100
Ti	Tr*	Tr	Tr
Cu	10	20	10
Al	100	100	100
Te	—	50	100
Cl	50	100	100
Si	100	200	200

* Trace

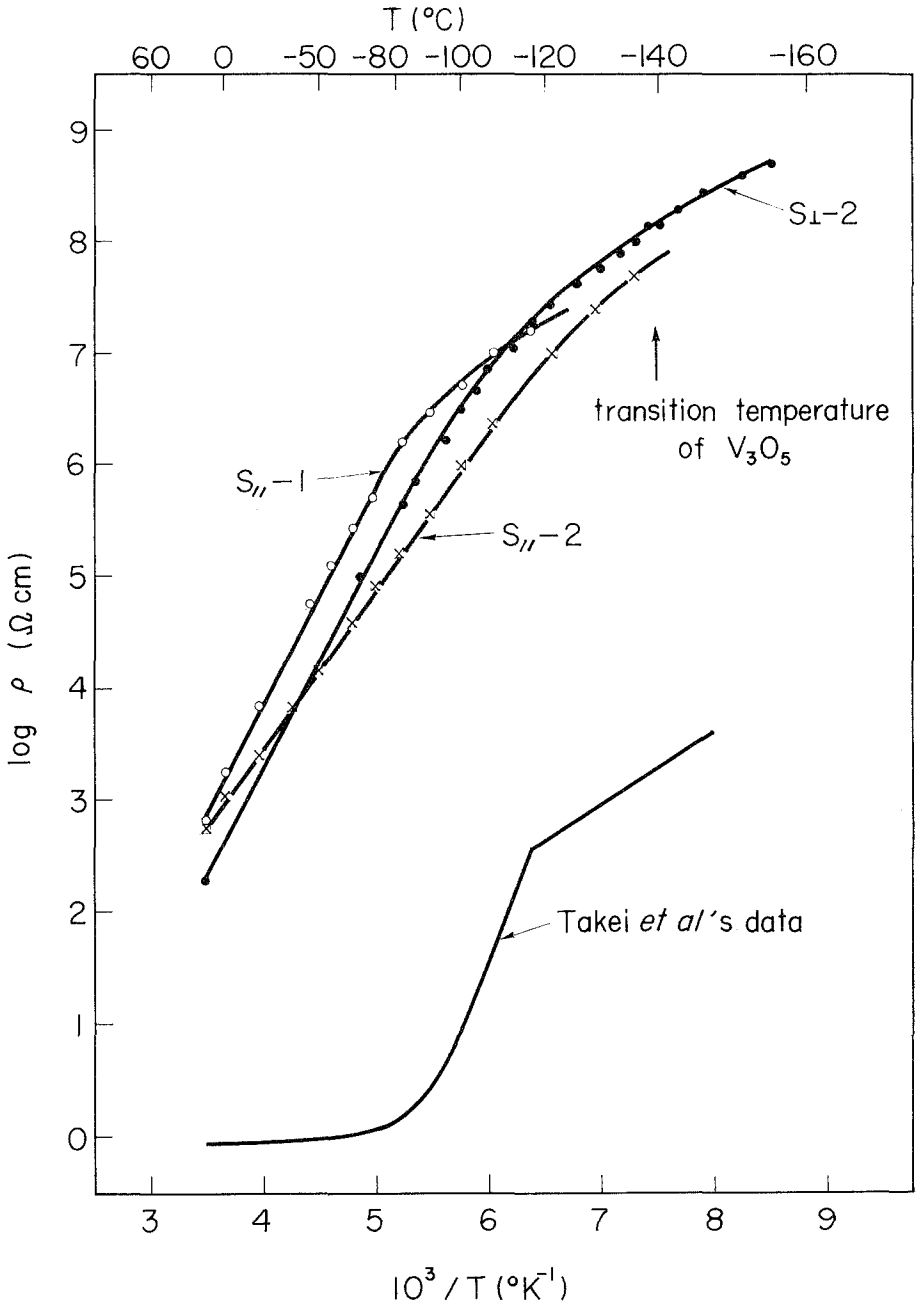

Fig. 6. Electrical resistivity versus temperature curves of V_3O_5. From 250°K to room temperature by four point method and below 250°K by two point method.

$S_{//}$ -1: Parallel to the growth axis of sample 1
$S_{//}$ -2: Parallel to the growth axis of sample 2
$S_{\perp}$ -3: Perpendicular to the growth axis of sample 2

The results of spectroscopic analysis are shown in Table 3. The little amounts of Te, Cl and Si were contained in single crystal.

2) Electrical properties

Electrical properties of as grown V_nO_{2n-1} crystals[20~23,25,26] are reviewed in paragraph (A), (B), (C), (D), (E), and (F) and summarized.

(A) V_3O_5

The electrical resistivity ρ of V_3O_5 was measured from room temperature to 120°K, as shown in Fig. 6. V_3O_5 has been clarified to be semiconductive in the measured temperature range. An activation energy of the electrical conduction was about 0.4 eV above 180°K and gradually decreased below 180°K. The anisotropy of ρ in the direction parallel and perpendicular to the growth axis was hardly observed.

Thermoelectric power α are plotted against temperature from room temperature to 200°C in Fig. 7. The negative sign of α indicated that V_3O_5 was n-type semiconductor. From the slope of the α-T curve, the Fermi energy measured from the

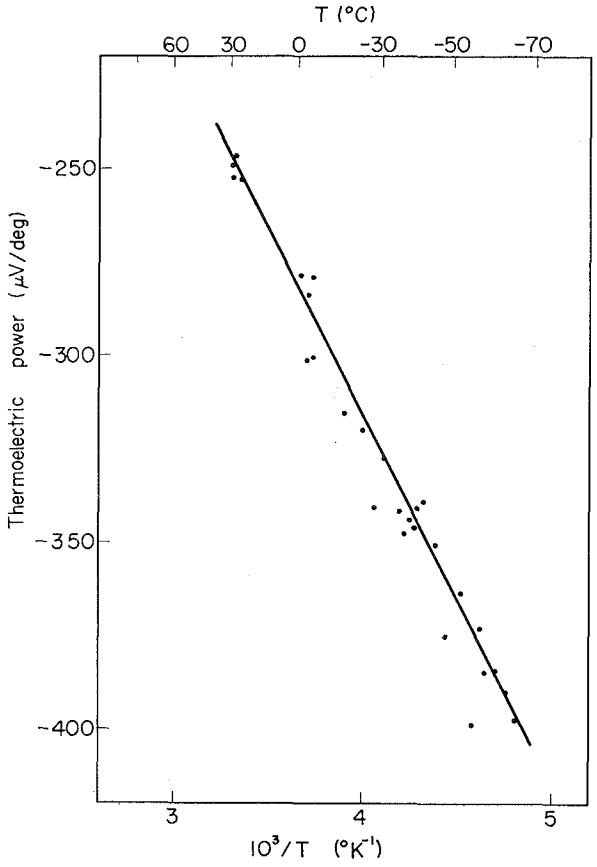

Fig. 7. Thermoelectric power versus temperature curve of V_3O_5.

bottom of conduction band was estimated to be about 0.1 eV. At 130°K, V_3O_5 had transition of the magnetic susceptibility χ, as shown in Fig. 3. However, the sharp anomaly on ρ-T curve was not observed. The metal-semiconductor transition at about 160°K reported by Takei *et al.*[14] could not be seen in the present experiment.

(B) V_4O_7

Figure 8 shows the temperature dependence of ρ. The V_4O_7 crystal underwent

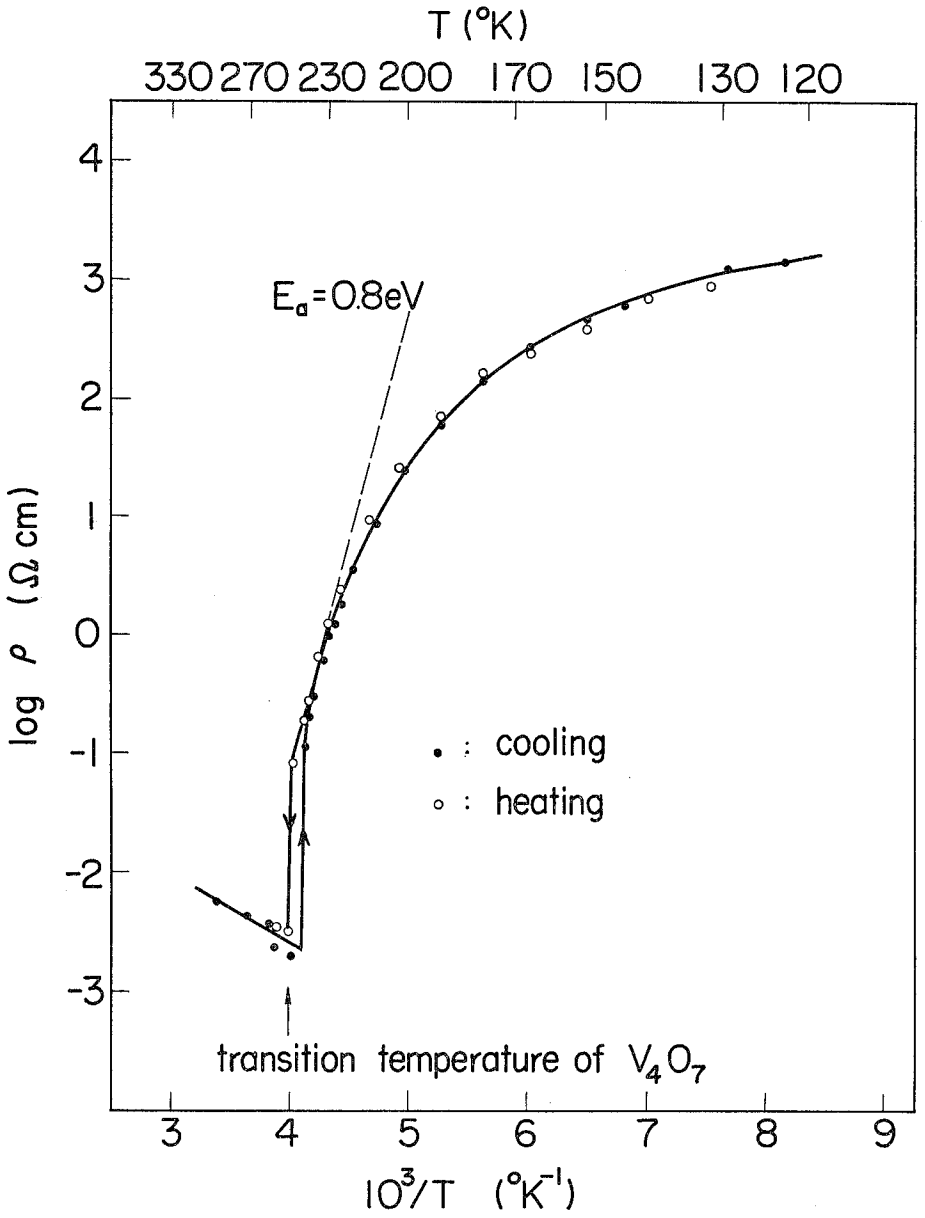

Fig. 8. Electrical resistivity versus temperature curves of V_4O_7.

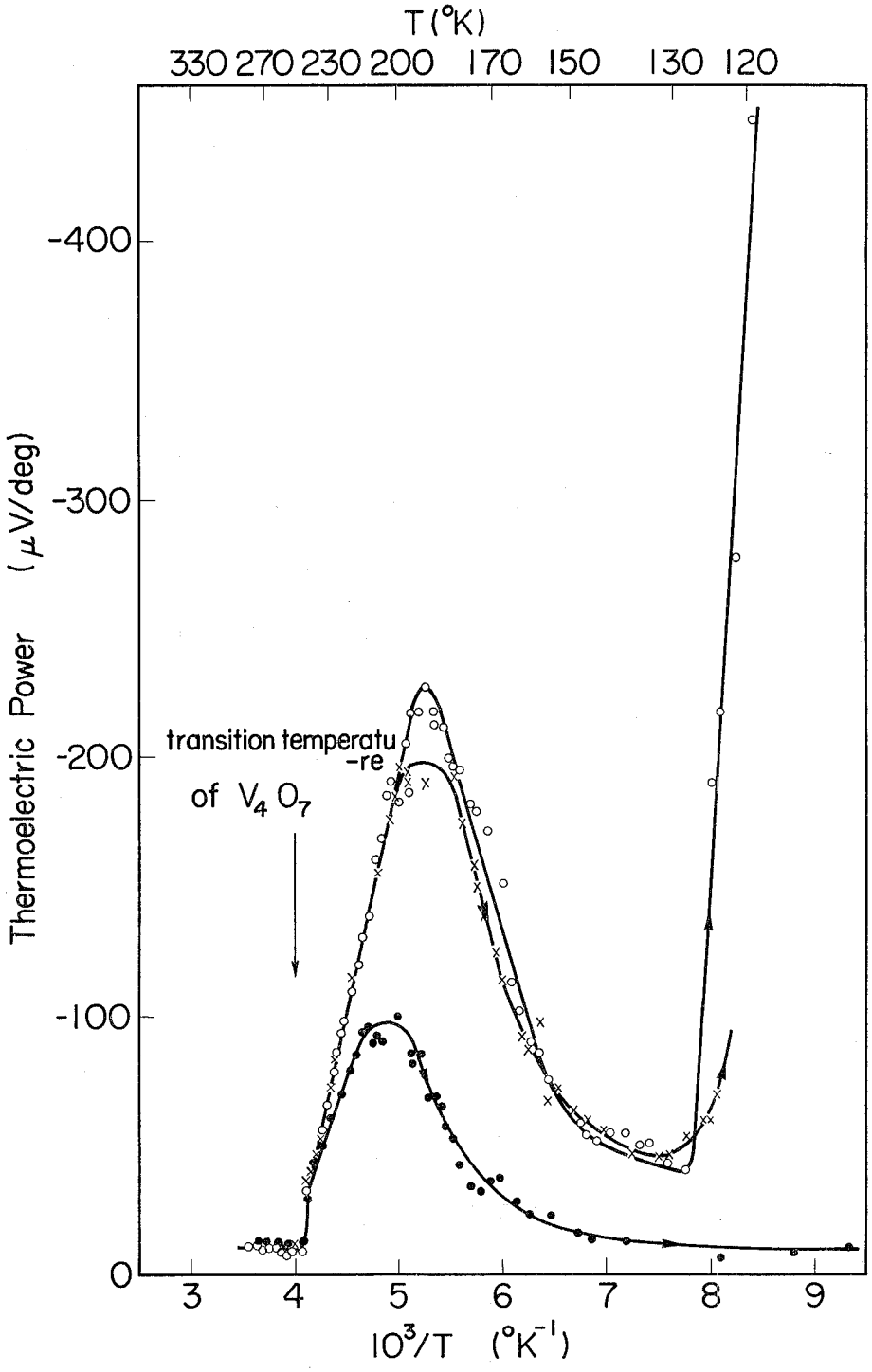

Fig. 9. Thermoelectric power versus temperature curves of V_4O_7.

a metal-semiconductor transition at 244°K on cooling. At the transition temperature Tt, ρ increased by about two orders of magnitude. Upon heating, a hysterisis of about 6°K was seen before ρ returned to the value of the metallic state. Transition temperature of ρ agreed approximately with that of χ shown in Fig. 3. An activation energy of the semiconducting state decreased from 0.8 eV to 0.1 eV with decreasing temperature. The temperature dependence of α is shown in Fig. 9. The absolute value of α suddenly jumped at Tt and gradually increased until about 195°K with

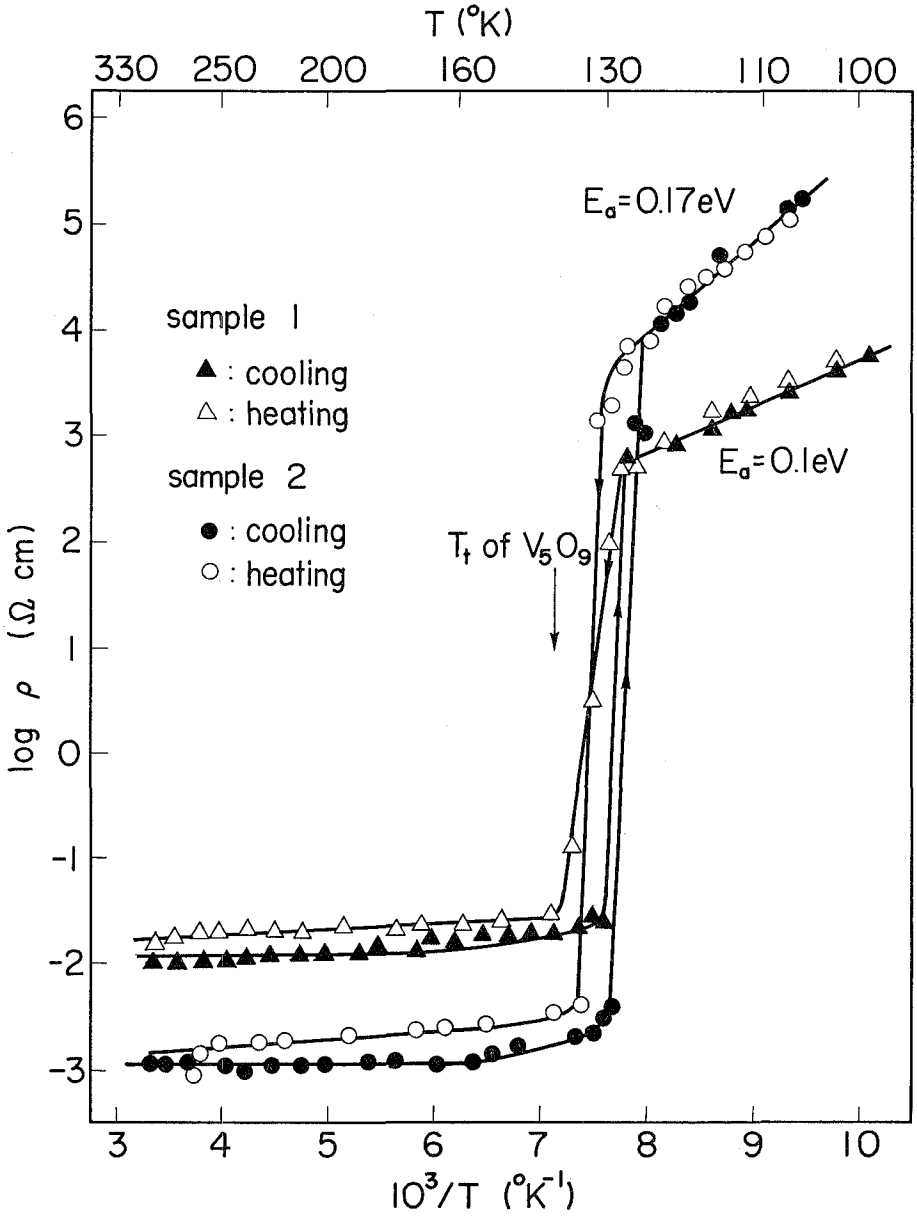

Fig. 10. Electrical resistivity versus temperature curves of V_5O_9.

decreasing temperature. From the slope, the Fermi energy measured from the bottom of conduction band was estimated to be about 0.15 eV. Below about 195°K, the absolute value of α decreased with decreasing temperature. In spite of the same temperature dependence of ρ, some sample showed the rapid increase of α below 120°K. The origin of these behaviors in α is not clear.

(C) V_5O_9

The V_5O_9 crystal underwent a metal-semiconductor transition at 129°K on cooling and at 135°K on heating, as shown in Fig. 10. This temperature corresponds with the transition temperature of χ. At the Tt, ρ increased by about five orders of magnitude. The value of and activation energy of semiconducting state showed a little difference between two samples. Increase in the absolute value of α was found below 130°K, as shown in Fig. 11 and the Fermi energy was estimated to be about 0.2 eV.

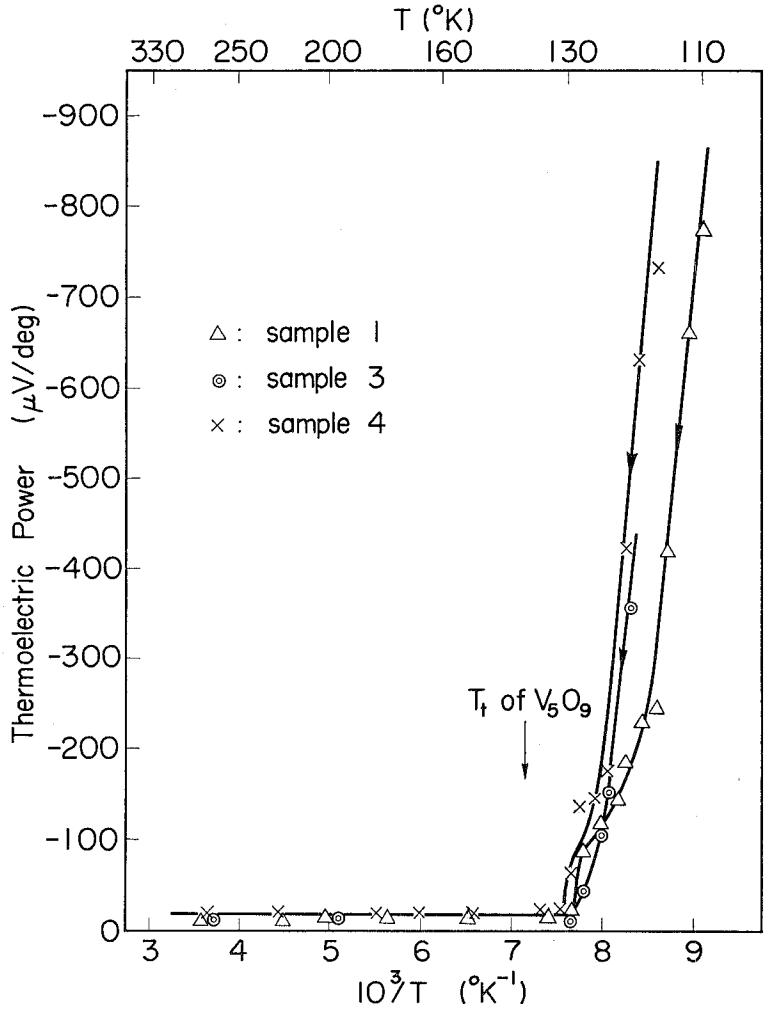

Fig. 11. Thermoelectric power versus temperature curves of V_5O_9.

(D) V_6O_{11}

The V_6O_{11} crystal had a metal-semiconductor transition at 175°K on cooling and at 177°K on heating, as shown in Fig. 12. An activation energy of semiconducting state was about 0.12 eV. As shown in Fig. 13, the absolute value of α abruptly increased at Tt, and decreased with decreasing temperature. Figure 14 shows the ρ-T curve of a crystal of C-2 which has two anomalies of V_5O_9 and V_6O_{11} on the χ-T curve. Two transitions corresponding to V_5O_9 and V_6O_{11} were also observed. This result shows that two phases coexist in a crystal.

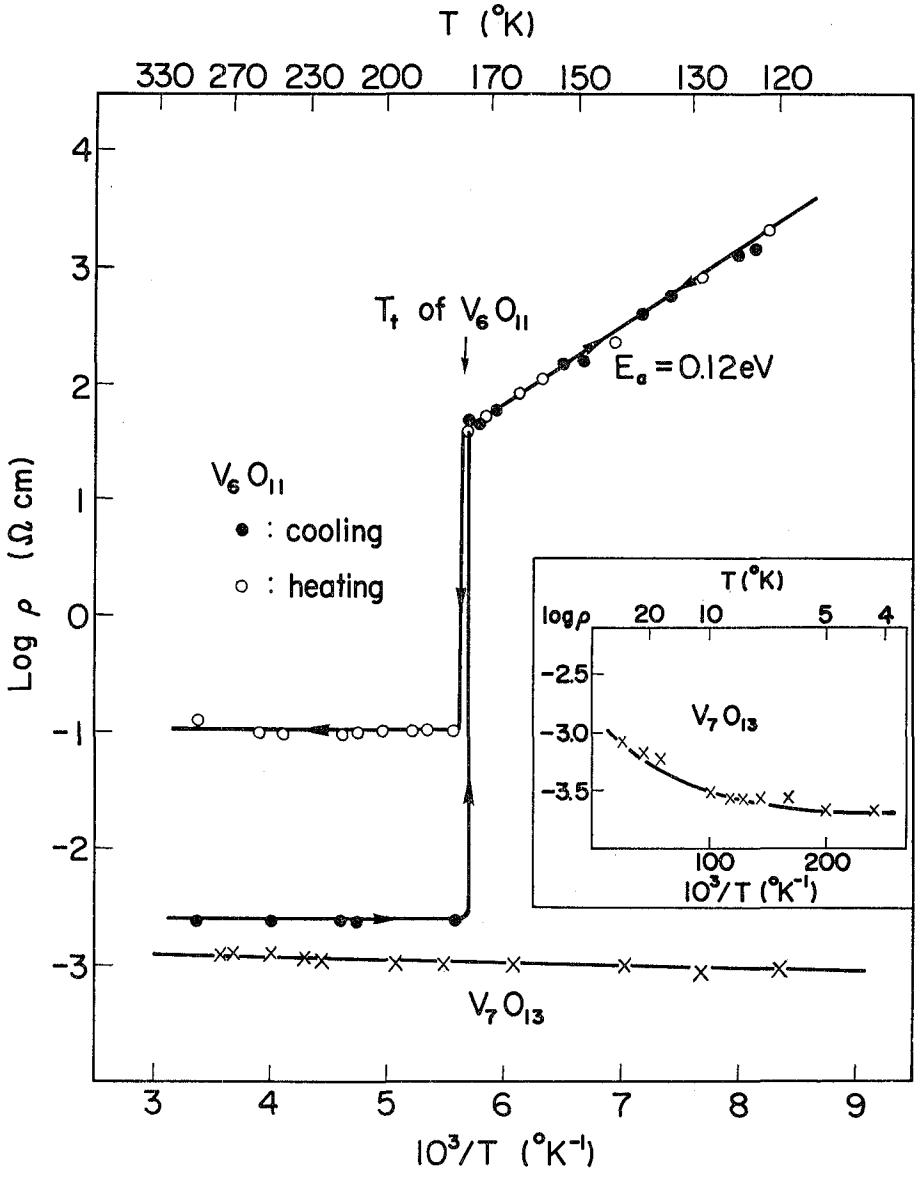

Fig. 12. Electrical resistivity versus temperature curves of V_6O_{11} and V_7O_{13}.

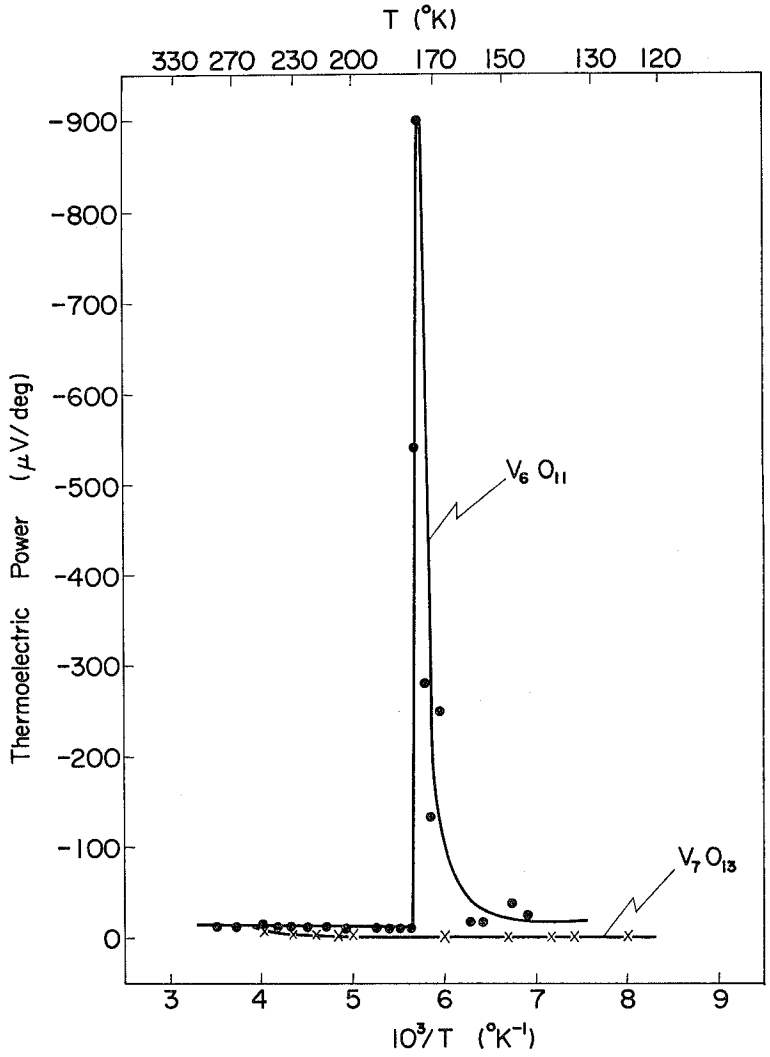

Fig. 13. Thermoelectric power versus temperature curves of V_6O_{11} and V_7O_{13}.

(E) V_7O_{13}

The conduction of V_7O_{13} was metallic over the temperature from 4.2°K to room temperature without transition, as shown in Fig. 12. Thermoelectric power was nearly constant in the temperature range from room temperature to 125°K, as shown in Fig. 13.

(F) V_8O_{15}

The temperature dependence of ρ on V_8O_{15} showed a metal-semiconductor transition at 70°K, as shown in Fig. 15. An activation energy just below Tt was about 0.13 eV. Below Tt, the abrupt increase in the absolute value of α was also observed, as shown in Fig. 16.

There were metal-semiconductor transitions in all the phases except V_7O_{15}. The

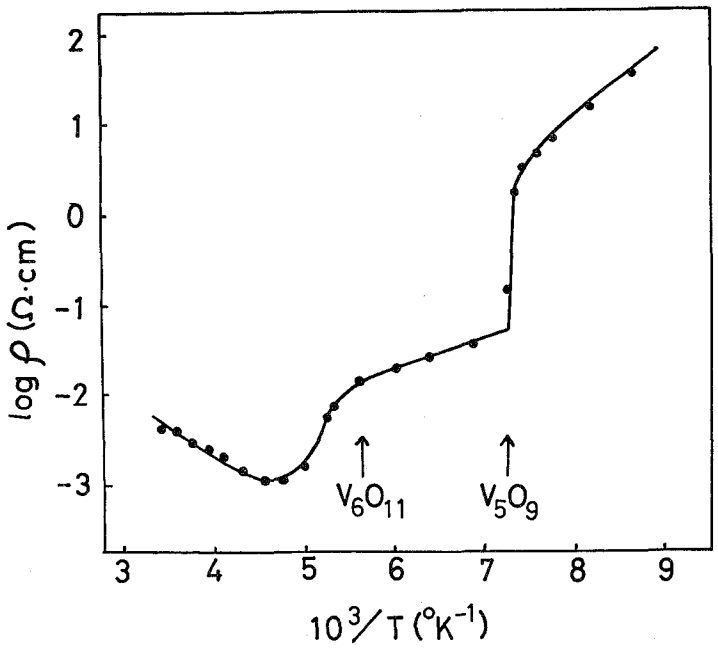

Fig. 14. Electrical resistivity versus temperature curve of the crystal consisting of two phases of V_5O_9 and V_6O_{11}.

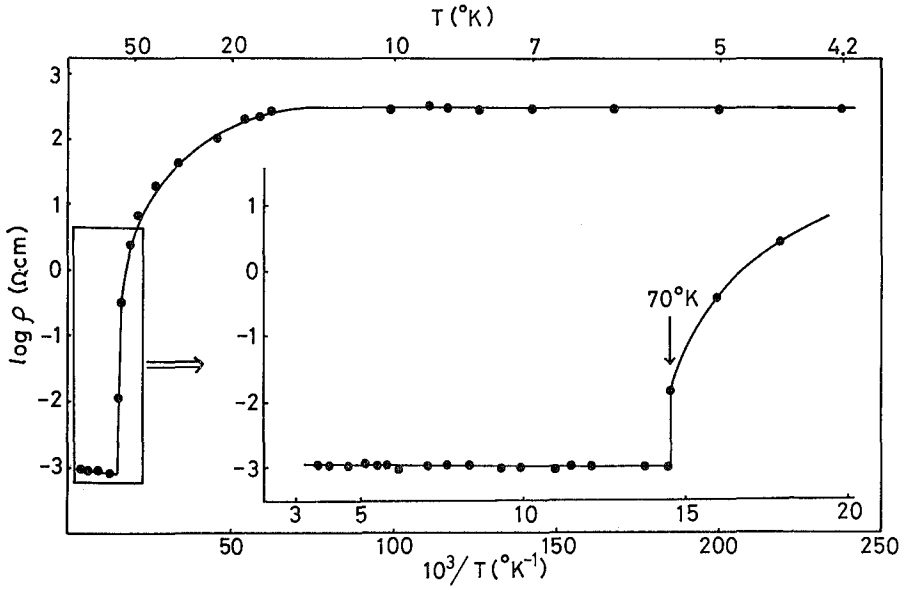

Fig. 15. Electrical resistivity versus temperature curve of V_8O_{15}.

list of various properties obtained in this experiment is given in Table 4. On all the metallic phases the electrical resistivities were $10^{-2}\sim19^{-3}$ Ω·cm and the thermoelectric powers were $0\sim-20$ μV/deg. On the semiconducting phase of V_4O_7 the activation energy of electrical resistivity increased with increasing temperature. This

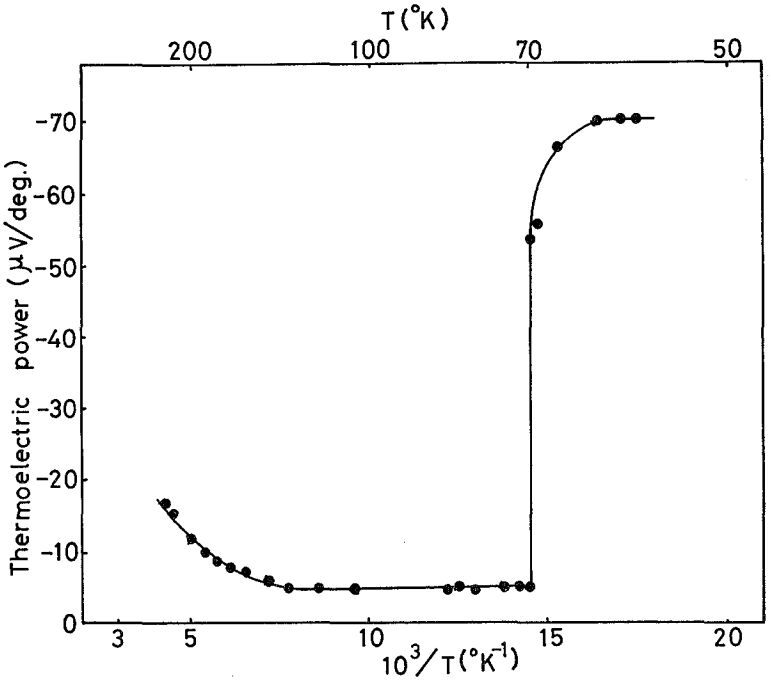

Fig. 16. Thermoelectric power versus temperature curve of V_8O_{15}.

Table 4. Electrical Properties of V_nO_{2n-1}.

	Tt of magnetic susceptibility (°K)	Characteristic of electrical conduction	Tt of electrical resistivity (°K) cooling	heating	Electrical resistivity of metallic phase (Ω·cm)	Thermoelectric power of metallic phase (μV/deg)	Activation energy of semiconducting phase (eV)	Fermi energy (eV)
V_3O_5	130±5 (133±5)	semicon. (n-type)	—	—	—		0.4	0.1
V_4O_7	250±2 (250±2)	metal-to-semicon. (n-type)	244	250	10^{-2}–10^{-3}	−10	0.8–0.1	0.15*
V_5O_9	135±3 (139±2)	metal-to-semicon. (n-type)	129	135	10^{-2}–10^{-3}	−20	0.1–0.2	0.2*
V_6O_{11}	170±3 (177±2)	metal-to-semicon. (n-type)	174	177	10^{-2}–10^{-3}	−10	0.12	
V_7O_{13}	—	metal	—	—	10^{-3}	0∼−1	—	—
V_8O_{15}	70±1 (—)	metal-to-semicon. (n-type)	—	70	10^{13}	−5∼−20	0.13	—

Kosuge's result is shown in bracket.

* Fermi energy measured just below Tt is shown.

behavior suggests that the intrinsic conduction by electrons which jump over the band gap is dominated near the transition temperature and the conduction at lower temperature becomes to be dominated by impurity levels in the band gap. The increase in

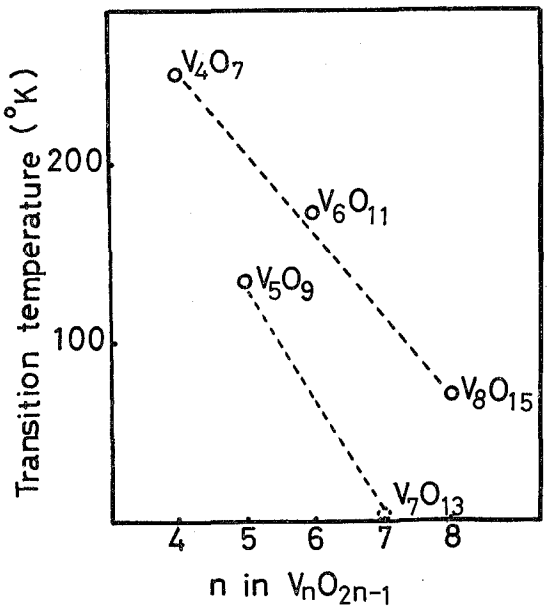

Fig. 17. Transition temperature versus n of V_nO_{2n-1}.

the thermoelectric power near the transition temperature also indicates the abrupt increase in electron concentration near the transition temperature. On all of the semiconducting phases, the electrical properties may be attributable to the impurity ions in the sample or the nonstoichiometry.

The temperature of metal-semiconductor transition of all the phases except V_3O_5 corresponded to that of the transition observed in magnetic susceptibility. Already, Kosuge[4] clarified for the magnetic transitions in V_4O_7 and V_5O_9 to be a transition from paramagnetic to paramagnetic. Measurement of the electrical resistivity showed a hysterisis loop. Moreover, the crackings of crystal which suggest the volume change of material at the transition were often observed. From these facts, the transitions would seem to be first order transitions like VO_2. However, the transition observed in V_3O_5 at 130°K, which had not a metal-semiconductor transition, may be from paramagnetic to antiferromagnetic.

Figure 17 shows the transition temperature of V_nO_{2n-1} versus n except n=3. On this figure, the following regularity may be pointed out for the transition temperature.

(1) Magnéli phases are classified into two groups having even and odd n by the transition temperature.

(2) The transition temperature decreases with increase of even and odd n, respectively.

Magnéli phases have triclinic structure based upon the rutile structure with the periodic shear plane. And so it may be considered that the introduction of shear plane gives the large influence on the transition. The relation of periodic structure of Magnéli phases with the transitions may cast some light on the mechanism of the transition in future.

ACKNOWLEDGMENTS

The authors are much indebted to Prof. Sukeji Kachi and Dr. Koji Kosuge for helpful discussions. Thanks are also due to Mr. Hideyuki Okinaka for making his electrical resistivity data and Prof. Nobuo Morimoto and Dr. Hiroyuki Horiuchi for making his x-ray data available to the authors.

REFERENCES

(1) G. Andersson, *Acta Chem. Scand.*, **8**, 1955 (1954).
(2) A. Burdese, *Annali. Chim.*, **47**, 785 (1957).
(3) G. Grossman, O. W. Proskurenko and M. Ss. Ariya, *Z. Anorg. allg. Chem.*, **305**, 121 (1960).
(4) K. Kosuge, *J. Phys. Chem. Solids*, **28**, 1613 (1967).
(5) S. Kachi and R. Roy, Second Quarterly Report on Crystal Chemistry Studies, Pennsylvania State University **4** December (1965).
(6) T. Katsura and M. Hasegawa, *Bull. Chem. Soc. Japan*, **40**, 561 (1967).
(7) T. Katsura and M. Hasegawa, Metallurgical Transactions **1** 363 (1970).
(8) H. Okinaka, K. Kosuge and S. Kachi, *Japan. J. Appl. Phys.*, **9**, 224 (1970).
(9) S. Andersson, *Acta Chem. Scand.*, **14**, 1161 (1960).
(10) S. Andersson and L. Jahnberg, *Arkiv for Kemi*, **21**, 413 (1963).
(11) S. Åsbrink, S. Friberg, A. Magnéli and G. Andersson, *Acta. Chem. Scand.*, **13**, 603 (1959).
(12) K. Kosuge, *J. Phys. Soc. Japan*, **22**, 551 (1967).
(13) S. Kachi, T. Takada and K. Kosuge, *J. Phys. Soc. Japan.*, **18**, 1839 (1963).
(14) H. Takei and S. Koide, *J. Phys. Soc. Japan*, **21**, 1010 (1966).
(15) T. Niemyski and W. Piekarczyk, *J. Cryst. Growth*, **1**, 177 (1967).
(16) Y. Bando, K. Nagasawa, Y. Kato and T. Takada, *Japan. J. Appl. Phys.*, **8**, 633 (1969).
(17) K. Nagasawa, Y. Bando and T. Takada, *Japan. J. Appl. Phys.*, **8**, 1262 (1969).
(18) K. Nagasawa. Y. Bando and T. Takada, *Japan J. Appl. Phys.*, **8**, 1267 (1969).
(19) K. Nagasawa, Y. Bando and T. Takada, *Japan. J. Appl. Phys.*, **9**, 407 (1970).
(20) H. Okinaka, K. Nagasawa, K. Kosuge, Y. Bando, T. Takada and S. Kachi, *J. Phys. Soc. Japan*, **27**, 1366 (1969).
(21) H. Okinaka, K. Nagasawa, K. Kosuge, Y. Bando, T. Takada and S. Kachi, *J. Phys. Soc. Japan*, **28**, 798 (1970).
(22) H. Okinaka, K. Nagasawa, K. Kosuge, Y. Bando, T. Takada and S. Kachi, *J. Phys. Soc. Japan*, **28**, 803 (1970).
(23) H. Okinaka, K. Nagasawa, K. Kosuge, Y. Bando, T. Takada and S. Kachi, *J. Phys. Soc. Japan*, **29**, 245 (1970).
(24) K. Nagasawa, Y. Bando, T. Takada, H. Horiuchi, Y. Tokonami and N. Morimoto, *Japan. J. Appl. Phys.*, **9**, 841 (1970).
(25) K. Nagasawa, *Mat. Res. Bull.*, **6**, (1971).
(26) H. Okinaka, K. Nagasawa, K. Kosuge, Y. Bando, T. Takada and S. Kachi, *Phys. Letters.*, **33A**, 370 (1970).
(27) T. Nakazono, *Nippon Kagaku Kaishi* (*in Japanese*), **42**, 761 (1921).
(28) H. Takeda and J. B. H. Donnay; Abst. Conf. on Computing Methods in Cryst. (1963) I-3 New York.
(29) H. Horiuchi, Y. Tokonami, N. Morimoto, K. Nagasawa, Y. Bando and T. Takada; to be Mat. Res. Bull., **6** (1971).